Original Research

Neonatal sevoflurane exposure induces long-term changes in dendritic morphology in juvenile rats and mice

Nemanja Useinovic[1]*, Michelle Near[1]*, Omar Hoseá Cabrera[1], Annalisa Boscolo[2,3], Andjelko Milosevic[1], Rachel Harvey[4], Adre Newson[1], Shelby Chastain-Potts[1], Nidia Quillinan[1,5†] and Vesna Jevtovic-Todorovic[1†]

[1]Department of Anesthesiology, University of Colorado Anschutz Medical Campus, Aurora, CO 80045, USA; [2]Institute of Anesthesia and Intensive Care, Padua University Hospital, Padua 35128. Italy; [3]Department of Medicine (DIMED), University of Padua, Padua 35128, Italy; [4]Oakland University William Beaumont School of Medicine, Rochester, MI 48309, USA; [5]Neuronal Injury and Plasticity Program, University of Colorado Anschutz Medical Campus, Aurora, CO 80045, USA
*These authors contributed equally to this paper.
†Equal senior author contributions.
Corresponding author: Nemanja Useinovic. Email: nemanja.useinovic@cuanschutz.edu

Impact Statement

Compelling preclinical evidence gathered over the past two decades has shown that neonatal exposure to general anesthetics caused significant acute neuronal death and long-term behavioral deficits. In addition, steadily accumulating clinical studies suggest that anesthetics may have deleterious effects on behavioral and cognitive development in children when administered during the first years of life. In this study, we used a well-established paradigm of anesthesia-induced neurotoxicity induced by sevoflurane, then examined the long-term changes in gene expression and dendrite branching pattern and complexity of pyramidal neurons in the subiculum. Our data suggest that a single 6-h exposure in PND7 rodents caused persisting changes in juvenile animals, manifesting via dysregulated expression of critical plasticity genes, increased dendritic complexity and dendritic spine density. These results further demonstrate our understanding of the histomorphological substrate behind the anesthesia-induced behavioral deficits and provide insight into the genetic dysregulation behind the observed morphological changes.

Abstract

General anesthetics are potent neurotoxins when given during early development, causing apoptotic deletion of substantial number of neurons and persistent neurocognitive and behavioral deficits in animals and humans. The period of intense synaptogenesis coincides with the peak of susceptibility to deleterious effects of anesthetics, a phenomenon particularly pronounced in vulnerable brain regions such as subiculum. With steadily accumulating evidence confirming that clinical doses and durations of anesthetics may permanently alter the physiological trajectory of brain development, we set out to investigate the long-term consequences on dendritic morphology of subicular pyramidal neurons and expression on genes regulating the complex neural processes such as neuronal connectivity, learning, and memory. Using a well-established model of anesthetic neurotoxicity in rats and mice neonatally exposed to sevoflurane, a volatile general anesthetic commonly used in pediatric anesthesia, we report that a single 6 h of continuous anesthesia administered at postnatal day (PND) 7 resulted in lasting dysregulation in subicular mRNA levels of cAMP responsive element modulator (*Crem)*, cAMP responsive element-binding protein 1 (*Creb1)*, and Protein phosphatase 3 catalytic subunit alpha, a subunit of calcineurin (*Ppp3ca)* (calcineurin) when examined during juvenile period at PND28. Given the critical role of these genes in synaptic development and neuronal plasticity, we deployed a set of histological measurements to investigate the implications of anesthesia-induced dysregulation of gene expression on morphology and complexity of surviving subicular pyramidal neurons. Our results indicate that neonatal exposure to sevoflurane induced lasting rearrangement of subicular dendrites, resulting in higher orders of complexity and increased branching with no significant effects on the soma of pyramidal neurons. Correspondingly, changes in dendritic complexity were paralleled by the increased spine density on apical dendrites, further highlighting the scope of anesthesia-induced dysregulation of synaptic development. We conclude that neonatal sevoflurane induced persistent genetic and morphological dysregulation in juvenile rodents, which could indicate heightened susceptibility toward cognitive and behavioral disorders we are beginning to recognize as sequelae of early-in-life anesthesia.

Keywords: General anesthesia, dendrite complexity, Sholl analysis, spine density, neurodevelopment, plasticity genes

Experimental Biology and Medicine **2023; 248: 641–655. DOI: 10.1177/15353702231170003**

Introduction

Exposure to general anesthesia (GA) during periods of neurodevelopment results in disruptions to synaptic circuitry, widespread apoptotic neurodegeneration, and neurotoxicity in brain regions critical to cognition and socio-emotional development.[1] Several histological studies have found that substantial cell death occurs in the brains of rodents[1,2] and nonhuman primates[3–6] following neonatal anesthetic exposure. Behavioral studies have further demonstrated that animals exposed to anesthesia in infancy have long-term impairments in multiple cognitive and affective domains lasting through adulthood.[1,7,8] Of particular concern is the growing body of clinical literature reporting neurodevelopmental abnormalities in children exposed to anesthesia in the neonatal period.[9–12]

Vulnerability to anesthesia-induced developmental neuroapoptosis coincides with synaptogenesis, a period of extensive synapse formation that establishes the communication networks supporting the brain's diverse cognitive repertoire.[13] Human synaptogenesis peaks in the third trimester of pregnancy with an estimated 40,000 new synapses formed every second.[13] In rodents, peak synaptogenesis occurs postnatally from the end of the first week of life until the early juvenile period.[14] Genetic, environmental, or pharmacological factors can dysregulate synapse formation within this critical window.[15,16] During the early neonatal period, GA is a potent pharmacological disruptor of synaptogenesis.[17] As millions of immature neurons are being apoptotically deleted from the developing brain during the aftermath of anesthesia exposure, billions more surviving neurons are exposed to a toxic milieu as they actively engage in a physiological process that are fundamental to normal cognitive and socio-affective functions. Thus, one plausible mechanism for neurodevelopmental abnormalities observed in rodents, nonhuman primates, and human children following neonatal anesthesia exposure is maladaptive changes in neuronal morphology, dendritic complexity, and connectivity.

Dendrites and dendritic spines function as the major input structures of neurons. The dendritic arbor increases the surface area over which neurons receive synaptic contact, while dendritic spines are preferential targets of excitatory synapses. This morphological arrangement allows dendrites to integrate and filter information from multiple populations of presynaptic neurons to ultimately regulate neuronal activity.[18] Dendrites and dendritic spines, the sites of excitatory synapses, also exhibit a high degree of homeostatic and activity-dependent synaptic plasticity,[19–22] the cellular basis of learning/memory and socio-affective development.

Previously, we reported pathological alterations to presynaptic axon terminals making postsynaptic contacts with subicular pyramidal neurons. These terminals had substantial reductions in neurotransmitter vesicles, swollen and damaged mitochondria, and redistribution of mitochondria away from the synapse.[23–25] Given that dendrites and dendritic spines are information integrators that exhibit activity-dependent plasticity,[19–21] they are likely to adapt to degraded presynaptic input from damaged axon terminals by rearranging microstructural features such as length, arborization, and spine density.[26,27] The morphological reorganization hypothesis is further supported by reports that neonatal anesthesia dysregulates genes and protein structures that are critical for dendritic architecture, maintenance, and plasticity.[28,29] Of relevance to this study is the increase in the immediate early gene *Arc*, we recently documented in the subiculum of juvenile rats anesthetized neonatally.[30] Overexpression of *Arc* is likely to modify transcription factors, neurotransmitter receptors, and signal transduction pathways that interact with *Arc* to regulate dendritic and synaptic stability.

In this study, we focus on the long-term impact of neonatal sevoflurane exposure on pyramidal neuron morphology and gene expression in subiculum, a hippocampal region known to be highly sensitive to anesthesia-induced developmental neuroapoptosis.[1,31] Sevoflurane is a common general anesthetic in neonatal and pediatric medicine, as well as a potent neuroapoptogen in the developing brain.[32–34] We exposed PND7 rat pups to a clinically relevant concentration of sevoflurane and collected tissue on PND28. We began by examining the expression of four genes that interact with *Arc* to regulate neuronal morphology and function: cAMP responsive element-binding protein 1 (*Creb1)*, cAMP responsive element modulator (*Crem*), glutamate N-methy-D-aspartate (NMDA) receptor subunit 2D (*Grin2D*), and calcineurin (Protein phosphatase 3 catalytic subunit alpha, a subunit of calcineurin *[Ppp3ca]*). Brains selected for histology were used for Golgi staining to assess neuronal morphology, dendrite complexity, and spine density in juvenile rats.

To further our morphological studies, we obtained Thy-1 enhanced green fluorescent protein (EGFP) heterozygous mice which spontaneously express in specific subsets of neurons. The high resolution and specificity of Thy-1 labeling allowed us to more accurately image detailed substructures of pyramidal neurons including branching patterns, basal dendritic arborization, and spinal density. Postnatal day (PND) 7 mice were exposed to the same regimen of sevoflurane as rat pups and were studied for morphological changes in subicular pyramidal neurons at PND28. Based on our previous data, our working hypothesis was that neonatal anesthesia would cause long-term dysregulation of genes critical to dendritic plasticity, which would manifest via alterations in dendritic complexity and spinal density of subicular pyramidal neurons.

Materials and methods

Animals

Sprague-Dawley rat pups were purchased from Envigo (Indianapolis, IN, USA). Litters of Thy1-EGFP mice (C57Bl/6 background) were purchased from Jackson Laboratories (Bar Harbor, ME, USA). Thy1-negative dams with positive sires were bred in-house to produce heterozygous offspring. All procedures were approved by the Institutional Animal Care and Use Committee at the University of Colorado Anschutz Medical Campus and the Office of Laboratory Animal Research Procedures were carried out in accordance with the Public Health Service Policy on Humane Care and Use of Laboratory Animals. Animals had *ad libitum* access to food and water and were maintained on a 14/10 h light/dark cycle.

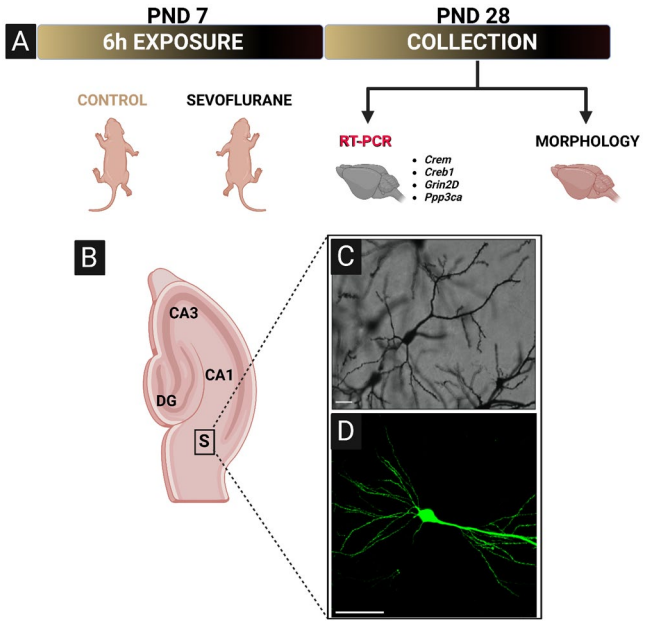

Figure 1. Schematic representation of experimental design, imaging region of interest, and representative photomicrographs. (A) PND7 rat or Thy1-EGFP mice were exposed to 6 h of sevoflurane anesthesia. After the exposure, animals were returned to their home cages and aged to PND28 before tissue collection. A subset of rat brains was selected for gene expression analysis of four genes (Crem, Creb1, Grin2D, and Ppp3ca) critical for neuronal development, learning, and memory. The remainder of rat and all of Thy1-EGFP mouse brains were selected and processed for histomorphological analyses. (B) Schematic of hippocampal formation defining the exact region of interest used for imaging purposes. (C) Representative 20× photomicrograph of optimized Golgi-Cox impregnation of subicular pyramidal neuron in rats. Scale bar = 100 µm. (D) Representative 40× photomicrograph of subicular pyramidal neuron in Thy1-EGFP mice, showing a much better resolution of small-diameter basal and apical dendritic branching. Scale bar = 50 µm.
Crem, cAMP responsive element modulator; *Creb1*, cAMP responsive element binding protein 1; *Grin2D*, Glutamate Ionotropic Receptor NMDA Type Subunit 2D; *Ppp3ca*, Protein phosphatase 3 catalytic subunit alpha, a subunit of calcineurin; S, subiculum; PND, postnatal day; EGFP, enhanced green fluorescent protein.

Sevoflurane anesthesia

For both mice and rats, litters comprised of male and female PND7 pups were exposed to either 6-h sevoflurane anesthesia (3% for 2 h and then 2.4% for 4 h) or carrier gas (30% oxygen) (Figure 1(A)). During experiments, pups were separated from their dam, placed in anesthesia chambers, and maintained at 35.5°C on homeothermic blanket systems (Harvard Apparatus, Holliston, MA, USA). Sevoflurane, oxygen, and carbon dioxide concentrations in anesthesia chambers were continuously monitored in real time (Datex Ohmeda Capnomac Ultima, Helsinki, Finland). Immediately upon cessation of the experiment, pups were tattooed for identification and were returned to home cages only when all anesthetized animals recovered righting reflex and responded to tail and toe pinch (approximately 30 min). Pups were then monitored for an additional 30 min to ensure that the dam nested and groomed the pups. Pups were weaned on PND21, aged to PND28, and then euthanized for tissue collection. In addition, mouse pups from Thy1 litters were also genotyped at PND21 and included in morphological analysis if positive for Thy1-EGFP.

Physiological parameters recorded during sevoflurane exposure in PND7 rat pups are summarized in Table 1.

Table 1. Physiological parameters in rats during 6 h of Sevoflurane Anesthesia. SpO_2, heart rate, and respiration were recorded in PND7 rat pups at the cessation of the 6-h experiments. As expected, 6-h sevoflurane anesthesia resulted in decreased heart rate and respiration compared with control pups. No signs of moderate (SpO_2 <95%) or severe (SpO_2 <90%) hypoxia were observed. Within 30 min of anesthesia cessation, anesthetized pups fully recovered and responded vigorously to tail and toe pinch.

Physiological parameters	Control	Sevoflurane
SpO_2	99.18 ± 0.08	97.34 ± 0.41
Heart rate (beats per minute)	376.5 ± 14.50	148.9 ± 4.42
Respiration (breaths per minute)	95.08 ± 3.58	34.33 ± 3.67

SpO_2, heart rate, and respiration were recorded for pups at the cessation of the 6-h experiment. Sevoflurane animals did not experience moderate (SpO_2 <95%) or severe (SpO_2 <90%) hypoxemia following 6 h of anesthesia. As expected based on our previous reports,[35,36] pups receiving 6-h sevoflurane had decreased heart rate and respiration compared with control pups that received only carrier gases. Thirty minutes after cessation of anesthesia, pups anesthetized with sevoflurane had recovered mobility and responded vigorously to tail and toe pinch.

Tissue collection

PND28 rat and mouse pups were deeply anesthetized with isoflurane and perfused with phosphate-buffered saline. Mouse pups were then perfused with 4% paraformaldehyde (pH 7.4), whereas rat brains were extracted and subjected to Golgi-Cox procedure (described below). Mouse brains selected for histology were rapidly extracted and fixed in 4% paraformaldehyde solution overnight at 4°C. The tissue was placed in 3% agarose and sectioned in coronal plane at 100 µm for mice and in transverse plane at 200-µm slices for rats (Leica VT 1200S vibratome, Leica Biosystems, USA). Slides corresponding to plates −2.92 to −3.16 mm from bregma in the mouse brain atlas[37] and subiculum corresponding to plates 111–113 of a rat brain atlas were used for imaging. Animals selected for molecular analyses were transcardially perfused with phosphate-buffered saline, decapitated, rapidly extracted left and right hippocampi were combined, and tissue was flash frozen in liquid nitrogen and stored at −80°C for until further use.

Real-time reverse transcription polymerase chain reaction

Real-time reverse transcription polymerase chain reaction (RT-PCR) was performed as previously described.[30] Briefly, subiculum tissue from 2 to 3 brains of the same sex and treatment was pooled, RNA was isolated from pooled samples using RNeasy Mini Kit (Qiagen, Hilden, Germany), and concentrations were determined spectrophotometrically (NanoDrop One; Thermo Scientific, Waltham, MA, USA). Reverse transcription was performed on 500 ng of RNA using iScript cDNA Synthesis Kit (Bio-Rad, Hercules, CA, USA), and concentrations were determined spectrophotometrically. Primers for Creb1, Crem, Grin2D, Ppp3ca, and Glyceraldehyde-3-Phosphate Dehydrogenase (GAPDH) were designed and purchased from Bio-Rad (Hercules, CA,

USA). Real-time RT-PCR reaction mixture consisted of 100 ng cDNA, 1X Sso Advanced Universal SYBR Green Supermix (Bio-Rad, Hercules, CA, USA), gene-specific 1× PrimPCR assay (Bio-Rad, Hercules, CA, USA), and nuclease-free water. The following PCR protocol was performed using CFX Connect Real-Time System (Bio-Rad; Hercules, CA, USA): 95°C for 2 m followed by 40 cycles of 95°C for 5°s and 60°C for 30°s, ending with a melting curve performed 65–95°C (0.5°C increments) at 5°s per step. PCR was performed in triplicate for Crem, Creb1, and Ppp3ca and in duplicate for Grin2d due to limited amount of RNA. Next, reference target and threshold cycle numbers were averaged. Relative expression of target gene was quantified by normalizing to GAPDH expression using the $2^{-\Delta(\Delta CT)}$ method. For statistical analysis, mRNA levels were expressed relative to the male vehicle group, which was assigned the value of 1.

Golgi staining

Impregnation stock solutions were prepared by dissolving 30 g of the following chemicals in 400 mL Milli-Q water (7.5% w/v): potassium dichromate, mercury chloride (heated to 37°C), and potassium chromate. All Golgi-Cox solution chemicals were purchased from Sigma-Aldrich (St. Louis, MO, USA). These stock solutions were then combined (first 1:1 potassium dichromate: mercuric chloride, followed by 5:2 mixture: potassium chromate) to produce the Golgi-Cox solution. After mixing the solution, the bottle was covered with aluminum foil and left to settle at room temperature for at least 48 h before use.

Extracted rat brains were washed with Milli-Q water and placed in 20 mL of Golgi-Cox solution. Every 24 h, brains were removed from solution, the container was washed twice with Milli-Q water, and 20 mL of fresh Golgi-Cox solution was added. This process was repeated for 10 consecutive days. After incubation in the Golgi-Cox solution, the brains were placed in 25% sucrose in phosphate-buffered saline at room temperature for 24–72 h. Next, the brains were air dried at room temperature in the dark, mounted in 3% agarose, sectioned in the transverse plane on a D.S.K. Microslicer DTK-1000 (Tokyo, Japan) at 200-µm thickness, and transferred to glass slides precoated with 1% porcine gelatin (Sigma-Aldrich, St. Louis, MO, USA). Sections were dried for a minimum of 24 h before being mounted on the slides.[38]

Light microscopy

Rat slides were imaged on a Nikon Eclipse E800 microscope (Nikon, Japan) using NIS Elements software (Nikon, Japan) by trained users blinded to experimental groups. Subicular pyramidal neurons were readily identified by their triangular soma, large apical dendritic trunk, and oblique branches covered with spiny protrusions. The Golgi method has been used to reliably analyze neuronal morphology, but a caveat of the method is that only a subset of neurons is impregnated. Therefore, neuronal reconstruction and morphometric analysis are only approximate as some dendrite branches and their spines may be hidden behind nearby cells. We strived to minimize these limitations by only selecting the neurons that met the following criteria: (1) Relative isolation from neighboring cells; (2) Dark and consistent impregnation of soma, apical dendrites, and spines; and (3) Untruncated apical dendrite arbor visible throughout the imaging field. From the population of neurons that met our inclusion criteria, a blinded experimenter randomly selected images for morphometric analyses. A total of 60 neurons (12 animals, 5 neurons per animal) were included in the analysis, with even distribution with regard to treatment and sex (15 neurons per treatment per sex). Images were taken at 20× magnification.

Immunofluorescent imaging

Slides containing Thy-1 positive mouse sections were imaged with an Olympus FV-1200 confocal laser scanning microscope (Olympus Corporation, Japan). Selection criteria to observe isolated pyramidal neurons consistently expressing EGFP were the same as for light microscopy previously described above. For Sholl analysis, 1024 × 1024 resolution images were obtained at 60× magnification with a stack size of 30–40 µm and a 0.5-µm step size. For spine density analysis, 1024 × 1024 resolution images were taken at 240× with a stack size of 5–10 µm and a 0.1-µm step size.

We assessed tissue from a total of 26 Thy-1 EGFP-positive mouse pups selected from 8 litters. The groups were composed of 12 control pups (n = 6 males and n = 6 females) and 14 pups exposed to sevoflurane (n = 7 males and n = 7 females). We excluded the neurons that did not meet our selection criteria, resulting in a total of 90 neurons for the control group (44 males and 46 females) and 100 neurons for sevoflurane group (50 males and 50 females). The most common exclusion criteria were as follows: truncated apical dendrite, overlap with neighboring neurons leading to inability to follow dendritic branches of individual neurons, and inconsistent expression of EGFP in distal branches.

Morphometric analyses

All measurements were performed in Fiji[39] and Imaris (v.9.9.1, Oxford Instruments, Abingdon, United Kingdom) software by an experimenter blinded to experimental groups. For analysis of dendritic branching, we used Simple Neurite Tracer (SNT), an open-source software plugin for FIJI with built-in Sholl Analysis.[40] SNT has demonstrated capability to accurately reconstruct neuron morphology,[41] as well as the sensitivity to determine morphology changes caused by experimental manipulations.[42,43] The experimenter ran the Analyze Skeleton plugin to determine number of branches, number of branch junctions, and average branch length in micrometer. We then performed Sholl analysis using a sampling radius of 5 µm. This radius was chosen based on preliminary linear plot data as the best compromise between continuous sampling and loss of Sholl plot curvature at radii of 10 µm or greater. Linear Sholl plot data were saved and reconstructed for analysis of dendritic complexity. For Sholl analysis, we also recorded sum intersections, max intersections, max intersections radius, enclosing radius, ramification index, and Sholl decay. Although all these parameters measure, in part, dendritic complexity, we used area under curve (AUC) of line plots as a single, summary measure of dendritic complexity.[41] We plotted number of intersections per 5 µm as a function of radial distance from the soma to

obtain line plots of each experimental condition and calculated AUC for each condition.

For spinal density analysis, we selected isolated secondary apical dendrite branches from pyramidal neurons in the CA1 regions and reconstructed the dendritic spines using Imaris software. A mask was created over the observed dendritic branches and spines using the surface tool with twice the thickness of the automated size to ensure complete coverage. The dendritic filaments were manually traced on the Masked EGFP channel with the filament path tool, and spines were marked by computer generated seed points. Thresholding values were set to fit the spine lengths and diameters as measured in slice mode, and seed points were removed around all starting points. To reduce inaccurate clusters of spines, duplicate seed points were manually deleted, and all spinal diameters were automatically adjusted. Spinal density was calculated as the total number of spines per 10-μm dendritic segment length.

Statistics

Power analysis and obtained effect sizes were calculated in G*Power (Heinrich Heine University Düsseldorf, Düsseldorf, Germany).[44] *Post hoc* power analysis suggested animal n = 4–6 per sex per treatment for rat gene expression and n = 5–10 per sex per treatment for mouse morphological analyses. For rat morphological analyses, power analysis suggested n = 8–12 per sex per treatment; therefore, we decided to combine males and females into single treatment groups. Data were analyzed and graphed using GraphPad Prism 9 (Dotmatics, Boston, Massachusetts). All data are expressed as mean ± SD and graphed as mean ± SEM. Treatment groups were compared using unpaired *t*-test or two-way ANOVA with treatment (control versus sevoflurane) and sex (male versus female) as factors. Multiple comparisons were computed via Sidak's *post hoc* tests. Significant treatment × Sex interactions were probed further with simple main effects to determine the primary driver of the interaction. The threshold for statistical significance was set at $\alpha = 0.05$.

Results

mRNA expression of synaptic plasticity genes in rat subiculum

Previously, we reported a significant dysregulation of immediate early genes, such as *Arc* and *JunB*, as a consequence of neonatal exposure to sevoflurane.[30] Due to the direct implications of *Arc* in a number of neurocognitive phenomena such as synaptic plasticity, long-term potentiation, memory consolidation, and synaptic weakening,[45] we first evaluated the expression of several genes critical to dendritic architecture, maintenance, and plasticity, that are known to interact with Arc: *Creb1*, cAMP responsive element modulator (*Crem*), glutamate NMDA receptor subunit 2D (*Grin2D*), and calcineurin (*Ppp3ca*).[45–49]

We found significant differences in subicular *Crem* mRNA levels as a result of treatment ($p < 0.01$), with no noticeable sex differences ($p = 0.43$) (Figure 2(A), left panel). Further analysis revealed a significant 63% downregulation of Crem mRNA following sevoflurane treatment in males ($p < 0.05$, Cohen's $f = 0.99$). Although we observed a similar, twofold reduction in Crem mRNA in sevoflurane-treated females compared with vehicle counterparts, this finding was not statistically significant ($p = 0.28$).

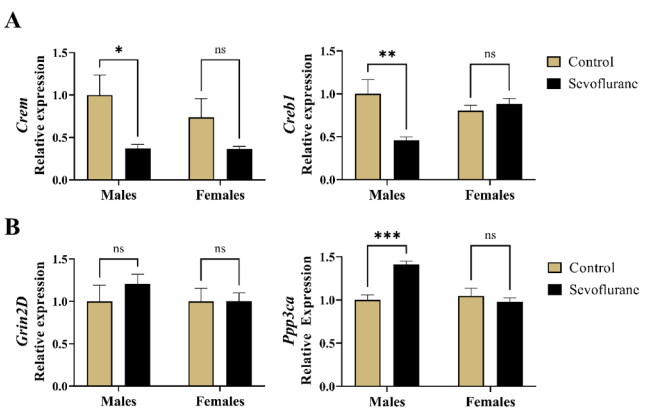

Figure 2. Long-term changes in hippocampal gene expression following neonatal administration of 6-h sevoflurane in rats. (A) *Crem* and *Creb1* are transcription factors that, in conjunction with Arc, regulate the expression of genes controlling neuronal morphology and function. Left panel: *Crem* hippocampal mRNA levels were significantly decreased following neonatal sevoflurane in males. Right panel: *Creb1* expression in the hippocampus was significantly downregulation in males neonatally exposed to sevoflurane. (B) *Grin2D* and *Ppp3ca* are regulated by Arc and implicated in learning and memory. Left panel: no change in gene expression of *Grin2D* was observed as a result of neonatal sevoflurane in either sex. Right panel: Neonatal sevoflurane significantly induced *Ppp3ca* expression in males compared with untreated controls. *$p < 0.05$; **$p < 0.01$; ***$p < 0.01$.
Crem, cAMP responsive element modulator; *Creb1*, cAMP responsive element-binding protein 1; *Grin2D*, Glutamate Ionotropic Receptor NMDA Type Subunit 2D; *Ppp3ca*, Protein phosphatase 3 catalytic subunit alpha.

Furthermore, we found the *Creb1* mRNA to be significantly dysregulated in response to treatment ($p < 0.05$) with no contributions of sex ($p = 0.23$). When we probed further with simple main effects, we observed a significant 54% downregulation of *Creb1* in males exposed to sevoflurane compared with controls ($p < 0.01$, Cohen's $f = 1.28$), but no differences between females ($p = 0.80$) (Figure 2(A), right panel).

Hippocampal expression of *Grin2D* (Figure 2(B), left panel), which encodes a subunit of the NMDA receptor, was seemingly unaffected by either the treatment ($p = 0.49$) or sex ($p = 0.51$). However, we did observe the effects of sevoflurane on *Ppp3ca* expression ($p < 0.05$), as well as the contribution of sex ($p < 0.01$) (Figure 2(B), right panel). Using the simple main effects to probe further, we concluded that the interaction was primarily driven by the 41% increase in *Ppp3ca* mRNA in males exposed to sevoflurane neonatally compared with unexposed controls ($p < 0.01$, Cohen's $f = 2.13$). On the contrary, no differences were found in females ($p = 0.79$).

Taken together, these data indicate a significant dysregulation in Crem, Creb1, and Ppp3ca gene expression in the subiculum following neonatal sevoflurane exposure, and that these findings were substantially more pronounced in the sevoflurane-exposed male rats.

Morphological evaluation of pyramidal neurons in rats and mice

Due to the dysregulated expression of genes of critical importance for dendritic architecture, maintenance, and plasticity,

Table 2. Histomorphological assessment of soma parameters of subicular pyramidal neurons in rats and mice. Soma area, height, and width were consistent across treatment and by sex.

		Males (M)	Females (F)	C versus S (males)	C versus S (females)
Soma morphology – Rat		Mean ± SD	Mean ± SD	Significance	
Soma area $(\mu m)^2$	Control (C)	226.90 ± 39.55	227.20 ± 98.10	$p = 0.47$	$p = 0.44$
	Sevoflurane (S)	257.30 ± 85.10	258.80 ± 64.60		
Soma height (μm)	Control	20.07 ± 2.64	20.20 ± 4.54	$p = 0.35$	$p = 0.62$
	Sevoflurane (S)	22.07 ± 5.28	21.53 ± 3.66		
Soma width (μm)	Control	15.13 ± 2.26	13.47 ± 2.80	$p = 0.96$	$p = 0.25$
	Sevoflurane (S)	15.40 ± 3.33	15.00 ± 2.51		
Soma morphology – Mouse		Mean ± SD	Mean ± SD	Significance	
Soma area $(\mu m)^2$	Control	149.80 ± 23.93	156.20 ± 27.44	$p = 0.57$	$p = 0.52$
	Sevoflurane (S)	154.40 ± 20.90	151.30 ± 22.44		
Soma height (μm)	Control	14.87 ± 2.49	15.84 ± 2.65	$p = 0.09$	$p = 0.93$
	Sevoflurane (S)	15.86 ± 2.19	15.68 ± 2.10		
Soma width (μm)	Control	12.15 ± 1.19	12.25 ± 1.23	$p = 0.97$	$p = 0.60$
	Sevoflurane (S)	12.10 ± 1.21	12.02 ± 1.37		

SD: standard deviation.

we then set out to determine whether there were accompanying alterations in the morphology of somata and dendritic arborization patterns of pyramidal neurons.

Golgi-stained and Thy1-positive pyramidal neurons in rat and mouse subicular sections, respectively, were readily identified due to their triangular soma and large apical dendritic arbor densely covered with dendritic spines, the sites of excitatory synapses on pyramidal neurons. The exact imaging region and representative images are shown in Figure 1(B), (C) and (D). Apical dendrites were prominent and easily identified in either Golgi or Thy1 preparations. In most cases, the initial segment of apical dendrites appeared devoid of dendritic spines, and extended upward roughly 50 μm before giving rise to secondary branches, densely covered with spinal protrusions.

However, the intricate pattern of basal dendrites' arborization on rat Golgi preparations was generally not discernible past the first generation of branches, while the Thy1-positive mouse neurons allowed for much greater resolution of branching patterns. In either preparation, there were no marked, qualitative differences in neuronal integrity between sevoflurane and control animals, such as corkscrewed and beaded apical dendrites and pyknotic soma indicative of ongoing neuroapoptotic cell death.

Quantitative assessment of soma parameters is summarized in Table 2. The soma surface area, height, and width were consistent across treatment and by sex in both rats and mice, which is to suggest that the somata of subicular pyramidal neurons in juvenile rats were unaffected by neonatal sevoflurane exposure and did not vary among sexes.

Quantitative assessment of dendritic complexity in rats

To begin to investigate the structural changes in apical dendritic arborization, we first performed Skeleton analysis to look for the changes in branching of apical dendrites in Golgi-stained subicular sections in rats (Figure 3(A)). We found the number of branches ($p < 0.05$, Cohen's $d = 0.63$) (Figure 3(A), left panel) and number of junctions ($p < 0.05$, Cohen's $d = 0.66$) (Figure 3(A), middle panel), but not the average branch length ($p = 0.19$) to be significantly increased in response to sevoflurane treatment (39.17 ± 24.23 branches and 19.70 ± 13.09 junctions) compared with anesthesia-naive controls (27.80 ± 8.63 branches and 13.23 ± 4.33 junctions). The 2:1 ratio of branches to junctions was consistent across the treatment groups, suggesting a predominant bifurcation branching pattern. We concluded that the apical dendritic arbor sustained significant changes toward increased ramification as a result of neonatal sevoflurane exposure.

Next, we employed the Sholl analysis to further analyze the complexity of apical dendritic arborization of subicular pyramidal neurons (Figure 3(B)). When we analyzed sum intersections, the total number of Sholl crossings at all Sholl radii (Figure 3(B), left panel), we observed a trend toward higher values in sevoflurane-treated animals (105.0 ± 55.62) compared with controls (88.60 ± 22.43), but this did not reach statistical significance ($p = 0.10$, Cohen's $d = 0.39$). However, we did find significantly increased values of max intersections, the maximum number of Sholl crossings at any Sholl radii (Figure 3(B), right panel) in juvenile rats neonatally exposed to sevoflurane (7.70 ± 2.68) when compared with untreated counterparts (6.23 ± 2.46) ($p < 0.05$, Cohen's $d = 0.57$). Additional Sholl parameters such as max intersections radius, enclosing radius, ramification index, and Sholl decay are summarized in Table 3.

Finally, we calculated the AUC as a single, overall measure of dendritic complexity for both experimental groups (Figure 4). The plotted Sholl curve revealed an obvious upward deflection following sevoflurane treatment compared with controls (Figure 4(A)). On statistical analysis (Figure 4(B)), we found that sevoflurane-exposed rats had significantly increased total AUC (685.30 ± 243.24) compared with anesthesia-naive controls (571.80 ± 172.86) ($p < 0.05$, Cohen's $d = 0.54$).

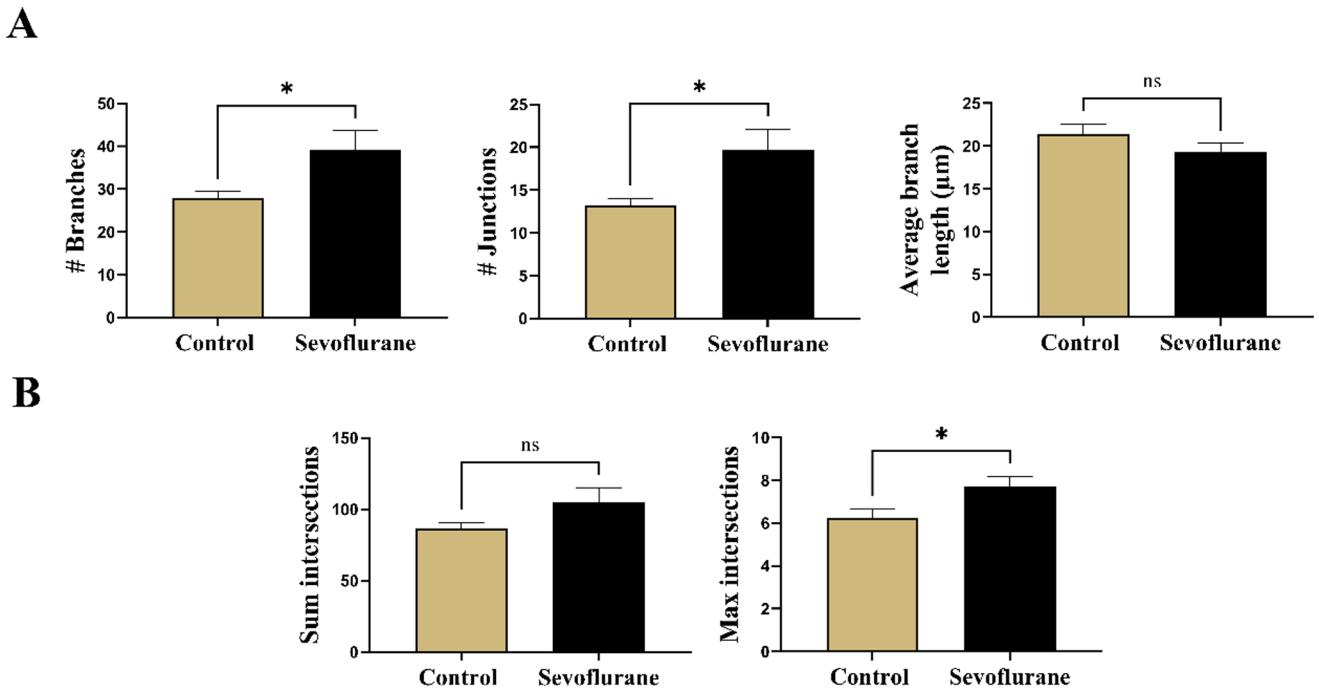

Figure 3. Quantitative assessment of apical dendrite complexity in Golgi-Cox impregnated subicular pyramidal neurons in rats. (A) Skeleton analysis of apical dendritic arborization. Left panel: total number of branches in apical dendritic arborization was significantly increased following neonatal sevoflurane. Middle panel: Total number of junctions, points from which multiple branches emanate, were similarly increased in apical arbor after sevoflurane compared with untreated controls. Right panel: However, no differences in average branch length were detected in either treatment groups. (B) Sholl analysis performed on apical dendritic arborization in 5-µm increments of Sholl radii. Left panel: Although a trend toward higher number of sum intersections, total number of Sholl crossings at all Sholl radii, was detected, statistical analysis revealed no significant difference. Right panel: Neonatal sevoflurane significantly increased Sholl max intersections, the highest number of Sholl crossings at any Sholl radii, indicating greater apical dendrite complexity in neonatally exposed rats to sevoflurane. *$p < 0.05$.

Table 3. Miscellaneous Sholl parameters of apical dendrite complexity of subicular pyramidal neurons in juvenile rats. No effects were observed as a result of treatment or between sexes.

Rat Sholl analysis		Mean ± SD	Significance (C versus S)
Max intersections radius	Control (C)	69.00 ± 38.45	$p = 0.82$
	Sevoflurane (S)	71.00 ± 30.01	
Enclosing radius	Control	163.20 ± 36.31	$p = 0.84$
	Sevoflurane (S)	165.8 ± 59.76	
Ramification index	Control	5.90 ± 2.74	$p = 0.16$
	Sevoflurane (S)	6.99 ± 3.17	
Sholl decay	Control	0.90 ± 0.95	$p = 0.85$
	Sevoflurane (S)	0.86 ± 0.92	

SD: standard deviation.

In summary, these data demonstrate significant long-term effects of neonatal sevoflurane exposure on reorganization of apical dendrites and indicate a shift toward higher levels of complexity when compared with age-matched, anesthesia-naive controls.

Quantitative assessment of dendritic complexity in mice

Due to the technical difficulties in performing the Golgi-Cox staining procedure on rat brains, leading to low number of biological replicates, we were underpowered to detect the potential sex differences. Recognizing the importance of sex as a biological factor, together with the need of better tools

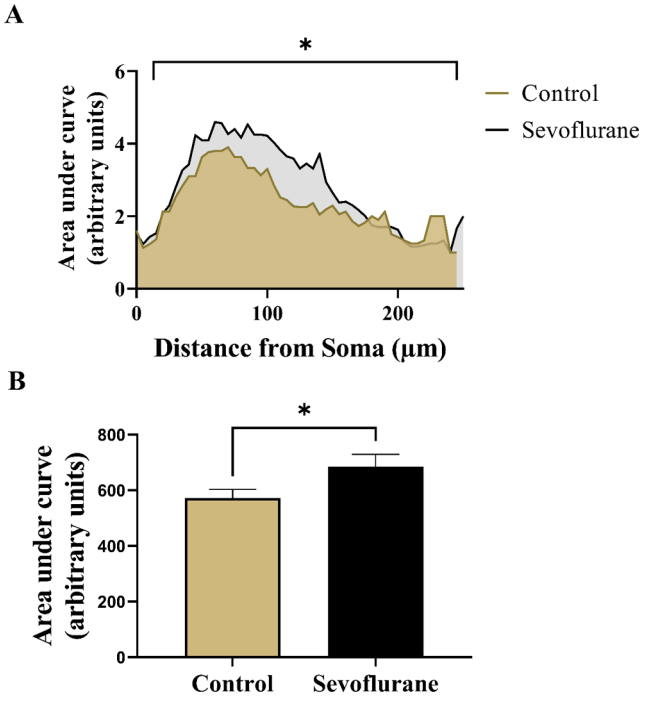

Figure 4. Quantitative analysis of overall apical dendritic complexity in Golgi-Cox impregnated subicular pyramidal neurons in rats. (A) Linear Sholl plots of number of intersections at Sholl radii in 5-µm increments from soma in sevoflurane-treated and anesthesia-naive rats. Neonatal sevoflurane caused a significant upward deflection of the corresponding Sholl curve, indicating increased apical dendritic complexity. (B) AUC analysis revealed significant increase in apical dendritic complexity in rats neonatally treated with sevoflurane. *$p < 0.05$. AUC, area under curve.

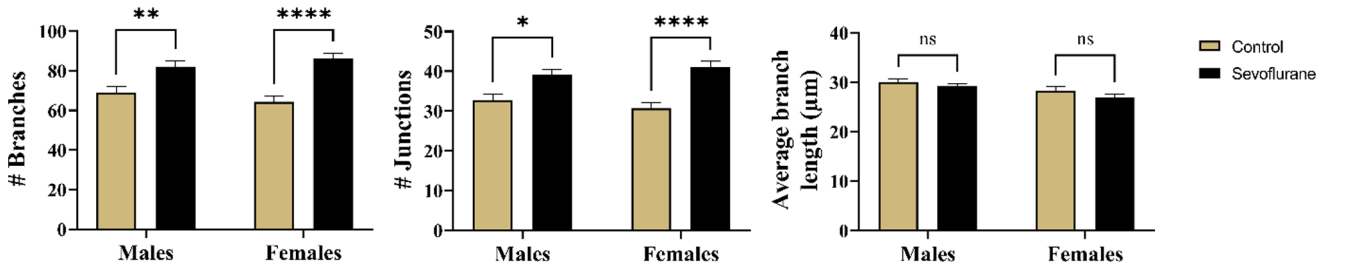

Figure 5. Skeleton analysis of arborization pattern of Thy1-EGFP expressing subicular pyramidal neurons in mice. Both apical and basal dendritic arbors were analyzed simultaneously to screen for gross alterations in branching pattern. Left panel: The overall increase in number of branches was substantially increased following neonatal sevoflurane in either sex, with more significant increase in sevoflurane-treated females. Middle panel: The number of junctions, points along dendrites with multiple emanating branches, exhibited similar pattern of increase following neonatal sevoflurane in both sexes, suggesting increase in overall branching of subicular pyramidal neurons. Right panel: No difference in average branch length was noted in any treatment groups in both sexes. $^{*}p < 0.05$; $^{**}p < 0.01$; $^{****}p < 0.0001$.
EGFP, enhanced green fluorescent protein.

to evaluate the basal dendritic arborization patterns, we next turned our attention toward Thy1-EGFP-positive mice as a means to answer these important questions.

We began our quantitative analysis of dendritic arborization in Thy1-EGFP mice by performing the skeleton analysis to probe for gross differences between treatment groups and sexes. We recorded the number of branches, number of junctions, and average branch length of multiple generations of dendrites, encompassing both the apical and the basal dendritic arbors (Figure 5). There was a strong main effect of treatment between groups ($p < 0.001$), but no differences were noted between sexes ($p = 0.91$). On further comparisons, it was revealed that sevoflurane-exposed males had significantly increased number of dendritic branches (82.16 ± 21.39 branches and 39.08 ± 10.48 junctions) compared with anesthesia-naive males (69.07 ± 19.81 branches and 32.77 ± 9.96 junctions) ($p < 0.01$, Cohen's $f = 0.32$ for branches and $p < 0.05$, Cohen's $f = 0.31$ for junctions) (Figure 5, left and middle panels). Surprisingly, these differences were found to be even more significant in females, with higher numbers of both measured parameters following neonatal sevoflurane (86.24 ± 18.82 branches and 41.14 ± 9.65 junctions) compared with vehicle counterparts (64.35 ± 19.40 branches and 30.70 ± 9.98 junctions) ($p < 0.0001$ for both, Cohen's $f = 0.57$ for branches and 0.53 for junctions) (Figure 5, left and middle panels). Finally, we observed no differences in average branch length in males ($p = 0.58$; 29.16 ± 4.10 versus 30.04 ± 4.77 for sevoflurane and controls, respectively) or in females ($p = 0.31$; 26.99 ± 4.46 versus 28.30 ± 5.21 for sevoflurane and controls, respectively) (Figure 5, right panel).

To further dissect the source of the observed differences in branching, we performed the Sholl analysis separately on basal and apical dendritic arbors in Thy1-positive mice (Figure 6). For the apical dendrites, we observed major differences between groups in response to treatment ($p < 0.001$) as the primary driving factor of significance. Sum intersections, the total number of crossings at Sholl radii, for apical dendritic branches was higher in treated males (139.40 ± 49.88) compared with untreated controls (110.20 ± 40.89) ($p < 0.01$, Cohen's $f = 0.32$) (Figure 6(A), left panel). Same was true for females, with significantly increased total number of crossings after sevoflurane (121.80 ± 46.85) compared with controls (95.85 ± 42.72) ($p < 0.05$, Cohen's $f = 0.29$) (Figure 6(A), left panel). In addition, the maximum number of crossings at

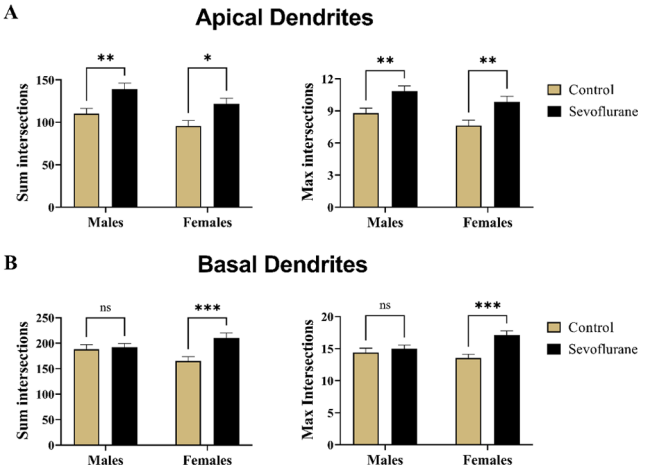

Figure 6. Quantitative assessment of dendritic complexity of Thy1-EGFP expressing mouse subicular by Sholl analysis. Dendrites of subicular pyramidal neurons were separated into apical and basal arbors with regard to their origin. (A) Sholl analysis of apical dendritic arborization revealed significantly higher level of complexity following neonatal sevoflurane treatment in both males and females, as evidenced by the measurement of sum intersections, total number of crossings at all Sholl radii (Left panel), and max intersections, highest number of Sholl crossings ay any radii (Right panel). The observed increase in complexity impacted sevoflurane-treated males more significantly than female counterparts. (B) On the contrary, increased complexity in basal dendritic arborization was detected only in sevoflurane-treated female mice, with significant increases in both sum intersections (Left panel) and max intersections (Right panel). No changes were observed as a result of treatment in males in either parameter. $^{*}p < 0.05$; $^{**}p < 0.01$; $^{***}p < 0.001$.
EGFP, enhanced green fluorescent protein.

any Sholl radii was also found to be higher following sevoflurane treatment, with both males (10.86 ± 3.47) and females (9.86 ± 3.71) displaying higher number of maximum intersections compared with anesthesia-naive male (8.80 ± 3.12) and female (7.60 ± 3.42) controls ($p < 0.01$ for both, Cohen's $f = 0.31$ and 0.32 for males and females, respectively) (Figure 6(A), right panel). Therefore, we concluded that apical dendrites undergo similar changes in both sexes following neonatal sevoflurane exposure.

We then took the same approach to analyzing the basal dendritic arborization (Figure 6(B)). Although treatment was the primary driving factor of significance for both the sum intersections and max intersections parameters ($p < 0.01$ for both), surprisingly this was true only in females. Sevoflurane-treated female mice had significantly higher values for

Table 4. Miscellaneous parameters of Sholl analysis performed separately on apical and dendritic arborization of subicular pyramidal neurons in juvenile mice. Neonatal sevoflurane induced significant increase in enclosing radius in males, indicating a wider apical dendritic arbor. Furthermore, ramification index in both males and females compared with controls, signifying higher ratio between maximum intersections and primary branches. No difference was noted in other parameters.

		Males (M)	Females (F)	C versus S (males)	C versus S (females)
Apical dendrite Sholl – mouse		Mean ± SD	Mean ± SD	Significance	
Max intersections radius	Control (C)	78.06 ± 18.56	80.19 ± 25.76	$p = 0.96$	$p = 0.29$
	Sevoflurane (S)	79.15 ± 19.97	86.57 ± 23.01		
Enclosing radius	Control	27.23 ± 4.07	28.17 ± 3.92	$^{*}p = \mathbf{0.04}$	$p = 0.72$
	Sevoflurane (S)	29.06 ± 3.47	28.74 ± 3.92		
Ramification index	Control	8.70 ± 3.20	7.63 ± 3.41	$^{**}p < \mathbf{0.01}$	$^{**}p < \mathbf{0.01}$
	Sevoflurane (S)	10.98 ± 3.40	9.86 ± 3.71		
Sholl decay	Control	0.93 ± 0.04	0.93 ± 0.04	$p = 0.06$	$p = 0.19$
	Sevoflurane (S)	0.91 ± 0.04	0.92 ± 0.04		
Basal dendrite Sholl – mouse		Mean ± SD	Mean ± SD	Significance	
Max intersections radius	Control	47.99 ± 16.19	41.86 ± 15.53	$p = 0.88$	$p = 0.39$
	Sevoflurane (S)	46.50 ± 16.05	45.90 ± 16.03		
Enclosing radius	Control	23.86 ± 3.11	22.61 ± 3.13	$p = 0.91$	$p = 0.65$
	Sevoflurane (S)	23.62 ± 2.87	23.12 ± 2.94		
Ramification index	Control	4.46 ± 2.41	3.82 ± 1.28	$p = 0.94$	$p = 0.10$
	Sevoflurane (S)	4.34 ± 1.37	4.52 ± 1.83		
Sholl decay	Control	0.97 ± 0.02	0.97 ± 0.01	$p = 0.78$	$p = 0.95$
	Sevoflurane (S)	0.97 ± 0.01	0.97 ± 0.01		

SD: standard deviation.

sum intersections (210.50 ± 68.39) and max intersections (17.10 ± 4.85) when compared with controls (165.20 ± 58.33 and 13.57 ± 3.95 for sum and max intersections, respectively) ($p < 0.001$ for both, Cohen's $f = 0.36$ and 0.40 for sum and max intersections, respectively) (Figure 6(B)). When males were compared with regard to sevoflurane treatment, we found their values of sum intersections (192.2 ± 52.42 versus 188.40 ± 59.02 for sevoflurane and controls, respectively) and max intersections (15.00 ± 4.07 versus 14.41 ± 4.28 for sevoflurane and controls, respectively) to be almost identical for both values ($p = 0.94$ and $p = 0.76$, respectively), indicating that rearrangement of basal dendritic arborization in response to neonatally administered sevoflurane was unique to the female sex (Figure 6(B)). Additional Sholl parameters such as max intersections radius, enclosing radius, ramification index, and Sholl decay are summarized in Table 4 for apical and basal dendrites separately.

To conclude our dendritic complexity analysis, we plotted the AUC for apical and basal Sholl crossings for both sexes separately. Such plots are visual representations of dendritic complexity that allow rapid evaluation and identification of experimental manipulations at a glance.[50] Peak amplitude of the Sholl plot is the measure of maximal dendritic complexity at a given distance from the soma. Shifts in the Sholl plot either leftward or rightward indicate changes to the overall complexity and branching of the dendritic arbor.[51]

When we plotted the total AUC for both the basal and apical dendrites combined (Figure 7(A)), we observed significant differences resulting from sevoflurane treatment ($p < 0.01$). *Post hoc* multiple comparisons revealed no differences in AUC values when sevoflurane males (1806 ± 555.86) were compared with male controls (1705 ± 524.49) ($p = 0.62$) (Figure 7(B), left panel). Although the Sholl curve indicated trend toward upward deflection in sevoflurane-treated males, most of this was concentrated in the apical rather than the basal dendritic region (Figure 7(A), left panel). On the contrary, we did find statistically significant differences in response to sevoflurane treatment in females (1791 ± 622.18) when compared with control counterparts (1425 ± 503.45) ($p < 0.01$, Cohen's $f = 0.32$) (Figure 7(B), left panel), which was clearly observable on the Sholl plot as an upward deflection of the curve representing sevoflurane-treated females, with balanced distribution in basal and apical dendritic regions (Figure 7(A), right panel).

To determine the relative contributions of basal versus apical dendritic arbor toward the upward deflection of the Sholl curve, we analyzed the area under these two regions separately. For basal dendrites, comparing the AUC values between sevoflurane-exposed (1059 ± 408) and unexposed males (1018 ± 427) revealed no differences ($p = 0.88$); however, females showed significantly higher AUC values in basal regions after sevoflurane (1084 ± 501) compared with controls (869 ± 399) ($p < 0.05$, Cohen's $f = 0.24$) (Figure 7(B), middle panel). When apical dendrites were analyzed in isolation, although there was a strong trend in both male (787 ± 377 versus 645 ± 304 for sevoflurane and control groups, respectively) and female mice (708 ± 369 versus 556 ± 306 for sevoflurane and control groups, respectively), we did not find statistically significant differences in neither male ($p = 0.09$, Cohen's $f = 0.21$) nor female mice ($p = 0.06$, Cohen's $f = 0.22$) (Figure 7(B), right panel).

Taken as a whole, our quantitative assessment of dendritic arborization revealed significant increase in dendritic complexity in juvenile mice following neonatal sevoflurane

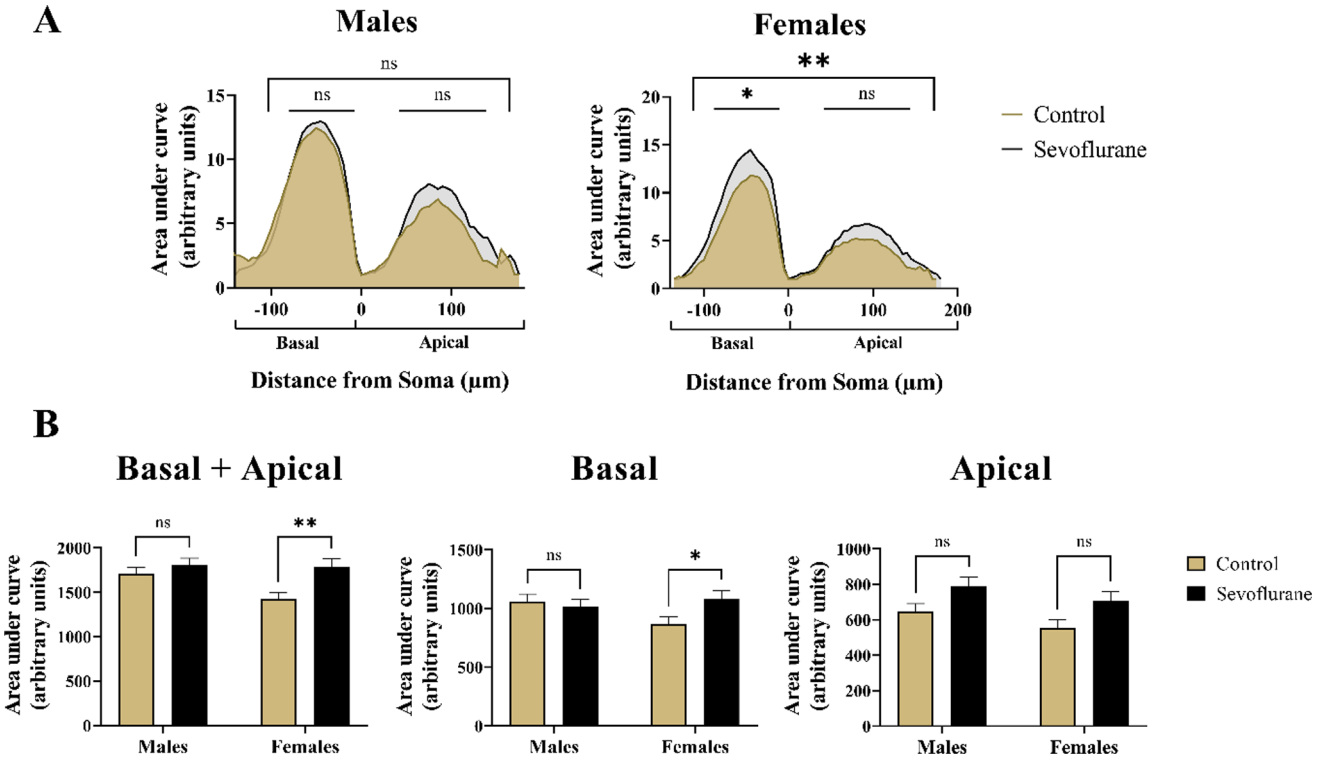

Figure 7. Summary measurement of differences in branching complexity of apical and basal dendritic arbors with regard to sex in Thy1-EGFP expressing mouse pyramidal neurons. (A) Visual inspection of Linear Sholl Plots, plotted as a function of distance from soma, suggested upward deflection following neonatal sevoflurane treatment. However, quantitative analysis revealed no significant differences in males (Left panel). In contrast, sevoflurane-treated females (Right panel) exhibited significant upregulation of overall Sholl plot, primarily in the basal dendritic arbor. Basal dendritic arborization was arbitrarily assigned negative values on the *x*-axis to differentiate it from the apical arbor. (B) Quantitative analysis of AUC revealed significantly higher values only in females following neonatal sevoflurane (Left panel). When basal arbor was analyzed in isolation, neonatally exposed females had significantly increased AUC values, whereas no differences were noted in males (Middle panel). Although the trend toward higher values was observed following sevoflurane in both males and females, no statistical significance was reached in the apical dendritic arbor (Right panel). *$p < 0.05$; **$p < 0.01$.
EGFP, enhanced green fluorescent protein.

exposure. This manifested as increases in the number of dendritic branches and junctions, increased total and maximum number of Sholl crossings, as well as upward deflections on Sholl plots, especially in females.

Quantitative assessment of dendritic spine density

Finally, we sought to determine whether the effects of neonatal exposure to anesthesia would also manifest as alterations in the density of the dendritic spines, the sites of excitatory synapses on pyramidal neurons. We decided to focus on the apical dendrites because (1) there were no indications of morphological changes in basal dendrites of sevoflurane-exposed males (see Figure 7), (2) apical dendrites are far more prominent in pyramidal neurons, allowing for easier and more accurate visualization and reconstruction, and (3) due to the presence of single apical dendrite on pyramidal neurons, it allowed for greater consistency in the selection criteria of the branches compared with basal arbor.

First, we performed semiautomated three-dimensional (3D) reconstruction of dendritic spines localized on the secondary apical dendrites, spanning the course of 20–90 µm long sampling segments (Figure 8(A)). The total number of dendritic spines per reconstructed segments were obtained and expressed per 10-µm branch length. Statistical analysis revealed a highly significant main effect of treatment in both males ($p < 0.001$) and females ($p < 0.001$) with no sexual dimorphism in either the control groups ($p = 0.37$) or the sevoflurane groups ($p = 0.94$) (Figure 8(B)). Multiple comparisons revealed that sevoflurane-exposed males (25.73 ± 4.78) had an 18% increase in the number of spines per 10 µm compared with unexposed controls (21.87 ± 3.35) ($p < 0.0001$, Cohen's $f = 0.47$). Likewise, we found females to also be affected, with sevoflurane-exposed females (25.47 ± 4.23) exhibiting a 23% increase in the number of spines per 10-µm length when compared with controls (20.75 ± 4.49) ($p < 0.0001$, Cohen's $f = 0.54$) (Figure 8(B)).

We, therefore, concluded that, in addition to causing alterations in dendritic complexity on the level of branching, neonatal sevoflurane induced substantial long-term increase in spine density on apical dendrites of subicular pyramidal neurons in a non-sex-specific manner.

Discussion

In this study, we examined the long-term impact of neonatal sevoflurane exposure on the expression of plasticity genes in subiculum, alongside the persisting effects on neuron morphology, dendritic structure, and complexity, as well as accompanying changes in spinal density on apical branches of subicular pyramidal neurons. By using a dose

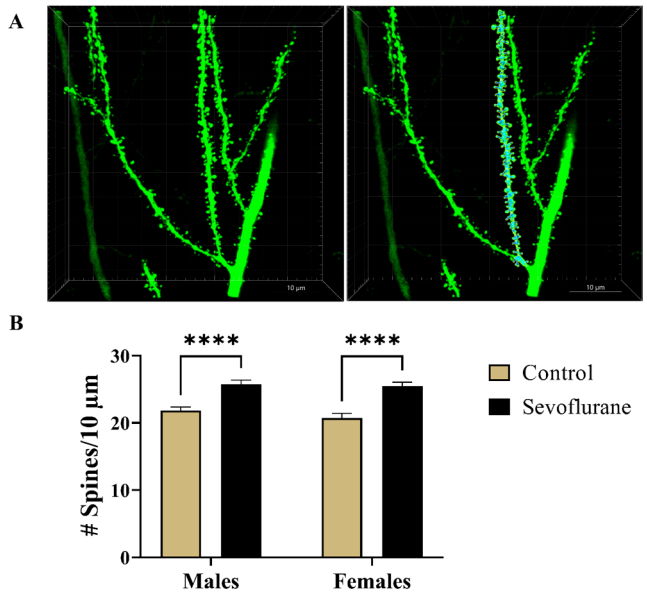

Figure 8. Spine density analysis of Thy1-EGFP-positive apical dendritic segments of subicular pyramidal regions in mice. (A) Representative photomicrographs of second generation dendritic branches covered with spines. Corresponding raw (Left panel) and the 3D-reconstructed (Right panel) images of dendritic spines are shown at 240× magnification. (B) Analysis of dendritic spine density, expressed as the number of spines per 10-µm long branch segments, revealed highly significant 18% and 23% increase in spine density in sevoflurane-exposed males and females, respectively. ****$p < 0.0001$. EGFP, enhanced green fluorescent protein.

and duration of sevoflurane which was shown to reliably and reproducibly cause apoptotic deletion of a substantial number of neurons when given at PND7,[33,34] we found that an early, single exposure to this clinically relevant anesthesia regimen[32] caused long-lasting remodeling of subicular dendritic arborization toward a more complex, hypertrophic morphology in juveniles while substantially increasing the number of dendritic spines. These alterations were accompanied by dysregulation of *Crem, Creb1*, and *Ppp3ca* genes that interact with *Arc* to influence dendritic morphology and neuronal function.[45,47,49] For yet unclear reasons, gene dysregulation was sexually dimorphic, with a 60% decrease in Creb1 mRNA and a 40% increase in Ppp3ca mRNA observed only in juvenile males exposed to sevoflurane in the neonatal period. Our observations add to the growing body of literature reporting that infant anesthesia has the ability to interfere with genetic regulation of neurons, as well as incur sex-specific neuropathological changes within the developing brain. These changes could be responsible, in part, for long-term impairments of neuronal development, synaptic communication, and cognitive function that we have previously reported.[1,23,52]

Traditionally, the subiculum has been viewed as the output of the hippocampus, funneling spatial information to cortical and subcortical regions for further processing and encoding.[53] However, recent evidence challenges the relay station hypothesis. Rather, the subiculum is a sophisticated computational unit that has a critical role in memory retrieval separate from hippocampus-dependent memory formation.[54,55] In addition, subiculum is exquisitely sensitive to neurotoxic action of early-in-life anesthesia, and acute apoptotic loss of subicular neurons following neonatal anesthesia exposure is well-documented,[24,31] as is the impact of anesthesia on the computational fidelity of the developing subiculum.[24,56,57] Microstructural rearrangements of dendritic morphology toward a hypertrophic phenotype, coupled with disturbances in gene expression, likely further alter subicular information processing capabilities. Dendrites and spines of subicular pyramidal neurons are responsible for the integration of glutamatergic excitatory signals in the subiculum. The maturation of these dendritic trees occurs mostly during early developmental stages through a pattern of slow growth of the dendrite succeeded by rapid extension and finally stabilization. Whereas the dendrites possess high remodeling capacity during early development, dendritic arbors in mature brains demonstrate significantly reduced plasticity but nonetheless remain essential for adequate nervous system performance.[58] Therefore, the proper wiring of neuronal circuitry during early development is of critical importance to a variety of cognitive and emotional processes. Given the central role of subiculum in a variety of neurocognitive processes, disturbances of connectivity during this crucial timeframe by general anesthetics and inability of mature neurons to achieve proper compensation may explain, at least in part, the diversity of functional outcomes observed later in life.

Dendritic hypertrophy may be driven by dysregulation of several genes working in concert. For example, many neuronal genes are subject to activity-dependent transcription, and anesthetics are powerful suppressors of neuronal activity. Therefore, anesthesia exposure is expected to influence gene expression at least acutely over the duration of anesthetic action.[59,60] But if the brain is exposed to anesthetics during sensitive periods of neurodevelopment – particularly synaptogenesis – the effects of anesthetics on neuronal gene expression appear to be chronic.[28,61] Dysregulation caused by neonatal anesthesia exposure encompasses an array of genes that themselves regulate the transcriptional activity of other genes (*Crem*, *Creb1*, *CREBBP*),[29] that serve as activity-dependent immediate early genes (*Arc*, *junB*, *c-Fos*),[29,30] and that control neuronal survival and morphology (Brain-derived neurotrophic factor [BDNF], synaptophysin, drebrin, [24, 53]).[28,62] Because the dendritic membrane is not a homogeneous structure along its length, aberrant production of proteins that are normally spatially targeted to dendritic compartments may lead to membrane instability, which in turn may lead to atrophy of certain generations of dendritic branches. In the intermediate and distal segments, loss of presynaptic excitatory information from afferent neurons killed by apoptosis and decreases in Crem may inhibit the activity of signaling pathways that maintain dendritic morphology. This reduction in appropriate synaptic input and gene expression may cause a compensatory morphological response that manifests as dendritic hypertrophy.

A parallel lever of neuronal dysfunction exists within the epigenome. Histone acetylation promotes gene expression by relaxing DNA chromatin, but anesthesia during the neonatal period substantially reduces the histone acetyltransferase activity of CREB-binding protein.[29] Furthermore, we recently reported that rats exposed to the same regimen of neonatal sevoflurane anesthesia as employed in this study

had substantial increases in Arc likely caused by widespread demethylation within the juvenile subiculum.[30] At the time, we postulated that *Arc* dysregulation could disrupt morphologic stability because *Arc* is directly involved in synaptic weakening via endocytosis of glutamate α-amino-3-hydroxy-5-methyl-4-isoxazolepropionic acid (AMPA) receptors from active synapses.[63,64] An important and concerning observation in our previous study was that genetic dysregulation of immediate early genes was heritable.[30] Male offspring that were never exposed to anesthesia but were born to females anesthetized as neonates had substantial increases in *Arc* and *junB* mRNA compared with males born to unexposed females. Whether epigenetic alterations contribute to dendritic hypertrophy observed in this study and are, therefore, also transgenerational remains to be determined.

Dysfunctions of both dendritic and spinal systems have been correlated with neurodevelopmental disorders such as schizophrenia and autism spectrum disorder (ASD) with alterations in dendritic morphology prominently occurring in the prefrontal cortex and hippocampus.[65] ASD is characterized by impairments in social interactions and persistent repetitive behaviors, and has been linked to a variety of environmental risk factors including exposure to infections, drugs, and toxins.[66] Although somewhat controversial, whether the use of early life anesthetics conveys increased risk of developing ASD remains an open question. A recent study found the correlation between the use of general anesthetics during cesarean section and ASD.[67] Furthermore, the risk was significantly higher in female children compared with males, especially for the severe form of ASD; however, a recent retrospective study failed to confirm the association between GA prior to age of 3 and ASD later in life after adjusting for birth weight and health status.[68] On the other side, the clinical evidence linking the early life GA and attention-deficit hyperactivity disorder (ADHD), a neuropsychological disorder impacting working memory, executive functioning, and impulsivity, has been steadily growing over the past decade. Multiple large-scale studies have found the significant risk to be conferred by the GA in the first years of life, after either single[69] or multiple anesthesia exposures.[70–72] With the prevalence of ADHD nearly doubled over the past two decades,[73] accurate and prompt identification of modifiable risk factors is more urgent than even before.

The apical and basal dendritic arborization of pyramidal neurons are separate systems with important differences in morphology, connectivity, and electrical properties, which strongly suggest different functionality.[18,74] Both apical and basal dendrites are densely covered with spines, sites of glutamatergic synapses of various morphology. Although both systems connect to a singular soma, there are important differences as to how the projections to these systems are integrated, both within the regional hippocampal circuitry and the inputs from thalamus and entorhinal cortex.[18,75] Whereas the basal dendrites participate primarily in intrahippocampal neuronal circuitry, mainly from CA3 pyramidal neurons, the majority of projections to apical dendritic arbor arrive from the thalamus and entorhinal cortex.[18] As the proapoptotic effects of volatile anesthetics on entorhinal cortex were previously reported in macaque neonates,[4] we speculate that the loss of excitatory input onto subicular apical dendrites from the entorhinal cortex via perforant path[76] could be responsible for the compensatory upregulation of dendritic complexity and spine density we observed in this study. Previous studies demonstrating sevoflurane-induced memory impairment at juvenile age suggest this compensatory mechanism is maladaptive, or not able to sufficiently compensate for the loss of neurons that occurs during the acute period following neonatal anesthetic exposure.[33]

In previous studies, apical dendrites in postmortem obtained cortical pyramidal neurons of subjects exhibiting symptoms of ASD expressed a higher density of dendritic spines[77] and abnormal dendritic branching.[58] ADHD symptomology is also correlated with disruptions to glutamate signaling through alterations in dendritic arborization and spinal density.[78] On the contrary, a previous study reported that the knockout of α7-subunit of nicotinic cholinergic receptors, which induces ADHD-like phenotype in experimental models,[79] predominantly targets basal dendrites, causing profound alterations in spine morphology, while inducing a significant increase in spine density of apical hippocampal CA1 pyramidal neurons in mice, which could act as histological markers of attention deficit-type disorders.[80] We postulate that the resulting changes observed from sevoflurane exposure in our current study could be a morphological marker for potential ADHD or autism-like symptoms. With roles in memory formation, cognition, and possibly emotional modulation,[55] the subiculum acts as an important regulator for behavior accounting for the resulting long-term deficits following GA exposure. Impairments to synaptic transmission in this area are likely to result in a notable decline in neurocognitive abilities.

Whether male sex is a risk factor in humans anesthetized as infants is an open question. In general, male infants are overrepresented in the anesthesia cohort of clinical studies, often at a ratio four times greater than that of female infants,[81,82] making it difficult to reliably identify any sex differences in cognition and behavior associated with neonatal anesthesia. Although the epidemiological studies have consistently reported higher prevalence of ADHD in males,[83,84] the gap seems to be steadily decreasing.[73] Despite the seemingly greater morphological alterations in dendritic complexity we observed in anesthesia-exposed females, particularly in the basal dendrites, it was only in males we detected changes in gene expression. Although it is tempting to speculate that this sexual dimorphism might represent a ceiling effect in males blocking sufficient compensatory dendritic branching, it is difficult to establish the causal relationship between gene expression and phenotype. Rather, it might also signify the failure of female rodents to trigger the necessary reparative genetic machinery necessary to offset the damage induced by anesthetics, therefore exposing the females to a potentially greater risk toward developing ADHD-like behavioral deficits as an outcome.

In summary, anesthesia-induced damage to the developing subiculum has morphologic and genetic hallmarks that may, in part, account for cognitive and socio-affective disturbances linked to neonatal anesthesia exposure. These sequelae parallel the cognitive and behavioral impairments in other disease states with similar morphological and genetic dysregulation. We believe that further studies aiming to put

these molecular and histomorphological changes into the context of developmental diseases are warranted and necessary. Finally, it is important that future preclinical and clinical investigations continue to incorporate sex as an important biological variable in such studies, with special consideration of the intricate interplay between gene expression and phenotypical changes.

AUTHORS' CONTRIBUTIONS

All authors participated in the design, interpretation of the studies and analysis of the data and review of the article; NU conducted the experiments, performed data quantification and interpretation and statistical analysis, and was responsible for writing the final version of the article; MN conducted the experiments, performed confocal imaging and spine density quantification, and helped in article writing; OHC participated in article writing and data interpretation; AB and RH performed the morphological quantification of Golgi-Cox impregnated rat tissue; AM contributed to the morphological analysis of Thy1-EGFP mouse morphological data; AN and SC-P performed the qPCR analyses of gene expression; SC-P optimized and performed the Golgi-Cox impregnation technique; NQ and VJT are senior authors responsible for study design, data analysis and interpretation, article preparation, and overall project supervision.

ACKNOWLEDGEMENTS

Parts of data were presented by Rachel Harvey at the American Society of Anesthesiologists National Conference 2019, Orlando, FL, in accordance with the Foundation for Anesthesia Education and Research's Medical Student Anesthesia Research Fellowship requirements.

DECLARATION OF CONFLICTING INTERESTS

The author(s) declared no potential conflicts of interest with respect to the research, authorship, and/or publication of this article.

FUNDING

The author(s) disclosed receipt of the following financial support for the research, authorship, and/or publication of this article: This work was supported by the Department of Anesthesiology at the University of Colorado Anschutz Medical Campus, Aurora, CO; Eunice Kennedy Shriver National Institute of Child Health and Human Development, Bethesda, MD [R01HD097990, R01HD044517, R01HD044517S, R21HD080281; F32HD101357]; National Institute of General Medical Sciences, Bethesda, MD [R01GM118197, R01GM118197-11S1], March of Dimes National Award, Crystal City, VA; CU Medicine Endowments, Aurora, CO; and the Foundation for Anesthesia Education and Research, Schaumburg, IL [MSARF-10-01-2019-Harvey].

ORCID ID

Nemanja Useinovic https://orcid.org/0000-0003-2788-7441

REFERENCES

1. Jevtovic-Todorovic V, Hartman RE, Izumi Y, Benshoff ND, Dikranian K, Zorumski CF, Olney JW, Wozniak DF. Early exposure to common anesthetic agents causes widespread neurodegeneration in the developing rat brain and persistent learning deficits. *J Neurosci* 2003;**23**:876–82
2. Cabrera OH, O'Connor SD, Swiney BS, Salinas-Contreras P, Manzella FM, Taylor GT, Noguchi KK. Caffeine combined with sedative/anesthetic drugs triggers widespread neuroapoptosis in a mouse model of prematurity. *J Matern Fetal Neonatal Med* 2017;**30**:2734–41
3. Creeley C, Dikranian K, Dissen G, Martin L, Olney J, Brambrink A. Propofol-induced apoptosis of neurones and oligodendrocytes in fetal and neonatal rhesus macaque brain. *Br J Anaesth* 2013;**110**:i29–38
4. Noguchi KK, Johnson SA, Dissen GA, Martin LD, Manzella FM, Schenning KJ, Olney JW, Brambrink AM. Isoflurane exposure for three hours triggers apoptotic cell death in neonatal macaque brain. *Br J Anaesth* 2017;**119**:524–31
5. Schenning KJ, Noguchi KK, Martin LD, Manzella FM, Cabrera OH, Dissen GA, Brambrink AM. Isoflurane exposure leads to apoptosis of neurons and oligodendrocytes in 20- and 40-day old rhesus macaques. *Neurotoxicol Teratol* 2017;**60**:63–8
6. Slikker W Jr, Zou X, Hotchkiss CE, Divine RL, Sadovova N, Twaddle NC, Doerge DR, Scallet AC, Patterson TA, Hanig JP, Paule MG, Wang C. Ketamine-induced neuronal cell death in the perinatal rhesus monkey. *Toxicol Sci* 2007;**98**:145–58
7. Raper J, Alvarado MC, Murphy KL, Baxter MG. Multiple anesthetic exposure in infant monkeys alters emotional reactivity to an acute stressor. *Anesthesiology* 2015;**123**:1084–92
8. Paule MG, Li M, Allen RR, Liu F, Zou X, Hotchkiss C, Hanig JP, Patterson TA, Slikker W Jr, Wang C. Ketamine anesthesia during the first week of life can cause long-lasting cognitive deficits in rhesus monkeys. *Neurotoxicol Teratol* 2011;**33**:220–30
9. Flick RP, Katusic SK, Colligan RC, Wilder RT, Voigt RG, Olson MD, Sprung J, Weaver AL, Schroeder DR, Warner DO. Cognitive and behavioral outcomes after early exposure to anesthesia and surgery. *Pediatrics* 2011;**128**:e1053–161
10. Ing C, Hegarty MK, Perkins JW, Whitehouse AJO, DiMaggio CJ, Sun M, Andrews H, Li G, Sun LS, von Ungern-Sternberg BS. Duration of general anaesthetic exposure in early childhood and long-term language and cognitive ability. *Br J Anaesth* 2017;**119**:532–40
11. Wilder RT, Flick RP, Sprung J, Katusic SK, Barbaresi WJ, Mickelson C, Gleich SJ, Schroeder DR, Weaver AL, Warner DO. Early exposure to anesthesia and learning disabilities in a population-based birth cohort. *Anesthesiology* 2009;**110**:796–804
12. Hu D, Flick RP, Zaccariello MJ, Colligan RC, Katusic SK, Schroeder DR, Hanson AC, Buenvenida SL, Gleich SJ, Wilder RT, Sprung J, Warner DO. Association between exposure of young children to procedures requiring general anesthesia and learning and behavioral outcomes in a population-based birth cohort. *Anesthesiology* 2017;**127**:227–40
13. Tau GZ, Peterson BS. Normal development of brain circuits. *Neuropsychopharmacology* 2010;**35**:147–68
14. Workman AD, Charvet CJ, Clancy B, Darlington RB, Finlay BL. Modeling transformations of neurodevelopmental sequences across mammalian species. *J Neurosci* 2013;**33**:7368–83
15. Qi C, Luo LD, Feng I, Ma S. Molecular mechanisms of synaptogenesis. *Front Synaptic Neurosci* 2022;**14**:939793
16. Xu J, Mathena RP, Xu M, Wang Y, Chang C, Fang Y, Zhang P, Mintz CD. Early developmental exposure to general anesthetic agents in primary neuron culture disrupts synapse formation via actions on the mTOR pathway. *Int J Mol Sci* 2018;**19**:2183
17. Jevtovic-Todorovic V. Developmental synaptogenesis and general anesthesia: a kiss of death. *Curr Pharm Des* 2012;**18**:6225–31
18. Spruston N. Pyramidal neurons: dendritic structure and synaptic integration. *Nat Rev Neurosci* 2008;**9**:206–21
19. Trachtenberg JT, Chen BE, Knott GW, Feng G, Sanes JR, Welker E, Svoboda K. Long-term in vivo imaging of experience-dependent synaptic plasticity in adult cortex. *Nature* 2002;**420**:788–94
20. McAllister AK. Cellular and molecular mechanisms of dendrite growth. *Cereb Cortex* 2000;**10**:963–73
21. Lendvai B, Stern EA, Chen B, Svoboda K. Experience-dependent plasticity of dendritic spines in the developing rat barrel cortex in vivo. *Nature* 2000;**404**:876–81
22. Hobbiss AF, Ramiro-Cortés Y, Israely I. Homeostatic plasticity scales dendritic spine volumes and changes the threshold and specificity of Hebbian plasticity. *iScience* 2018;**8**:161–74

23. Lunardi N, Ori C, Erisir A, Jevtovic-Todorovic V. General anesthesia causes long-lasting disturbances in the ultrastructural properties of developing synapses in young rats. *Neurotox Res* 2010;**17**:179–88
24. Sanchez V, Feinstein SD, Lunardi N, Joksovic PM, Boscolo A, Todorovic SM, Jevtovic-Todorovic V. General anesthesia causes long-term impairment of mitochondrial morphogenesis and synaptic transmission in developing rat brain. *Anesthesiology* 2011;**115**:992–1002
25. Boscolo A, Milanovic D, Starr JA, Sanchez V, Oklopcic A, Moy L, Ori C C, Erisir A, Jevtovic-Todorovic V. Early exposure to general anesthesia disturbs mitochondrial fission and fusion in the developing rat brain. *Anesthesiology* 2013;**118**:1086–97
26. Berry RH, Qu J, John SW, Howell GR, Jakobs TC. Synapse loss and dendrite remodeling in a mouse model of glaucoma. *PLoS ONE* 2015; **10**:e0144341
27. Flores G, Alquicer G, Silva-Gómez AB, Zaldivar G, Stewart J, Quirion R, Srivastava LK. Alterations in dendritic morphology of prefrontal cortical and nucleus accumbens neurons in post-pubertal rats after neonatal excitotoxic lesions of the ventral hippocampus. *Neuroscience* 2005;**133**:463–70
28. Obradovic AL, Atluri N, Dalla Massara L, Oklopcic A, Todorovic NS, Katta G, Osuru HP, Jevtovic-Todorovic V. Early exposure to ketamine impairs axonal pruning in developing mouse hippocampus. *Mol Neurobiol* 2018;**55**:164–72
29. Dalla Massara L, Osuru HP, Oklopcic A, Milanovic D, Joksimovic SM, Caputo V, DiGruccio MR, Ori C, Wang G, Todorovic SM, Jevtovic-Todorovic V. General anesthesia causes epigenetic histone modulation of c-Fos and brain-derived neurotrophic factor, target genes important for neuronal development in the immature rat hippocampus. *Anesthesiology* 2016;**124**:1311–27
30. Chastain-Potts SE, Tesic V, Tat QL, Cabrera OH, Quillinan N, Jevtovic-Todorovic V. Sevoflurane exposure results in sex-specific transgenerational upregulation of target IEGs in the subiculum. *Mol Neurobiol* 2020;**57**:11–22
31. Rizzi S, Carter LB, Ori C, Jevtovic-Todorovic V. Clinical anesthesia causes permanent damage to the fetal guinea pig brain. *Brain Pathol* 2008;**18**:198–210
32. Lerman J. Sevoflurane in pediatric anesthesia. *Anesth Analg* 1995;**81**: 4–10
33. Satomoto M, Satoh Y, Terui K, Miyao H, Takishima K, Ito M, Imaki J. Neonatal exposure to sevoflurane induces abnormal social behaviors and deficits in fear conditioning in mice. *Anesthesiology* 2009;**110**: 628–37
34. Sun Z, Satomoto M, Adachi YU, Kinoshita H, Makita K. Inhibiting NADPH oxidase protects against long-term memory impairment induced by neonatal sevoflurane exposure in mice. *Br J Anaesth* 2016; **117**:80–6
35. Tesic V, Joksimovic SM, Quillinan N, Krishnan K, Covey DF, Todorovic SM, Jevtovic-Todorovic V. Neuroactive steroids alphaxalone and CDNC24 are effective hypnotics and potentiators of $GABA_A$ currents, but are not neurotoxic to the developing rat brain. *Br J Anaesth* 2020;**124**:603–13
36. Useinovic N, Maksimovic S, Liechty C, Cabrera OH, Quillinan N, Jevtovic-Todorovic V. Systemic inflammation exacerbates developmental neurotoxicity induced by sevoflurane in neonatal rats. *Br J Anaesth* 2022;**129**:555–66
37. Paxinos G, Franklin K. *Paxinos and Franklin's the mouse brain in stereotaxic coordinates*. San Diego, CA: Academic Press, 2001
38. Zhong F, Liu L, Wei JL, Dai RP. Step by step Golgi-Cox staining for cryosection. *Front Neuroanat* 2019;**13**:62
39. Schindelin J, Arganda-Carreras I, Frise E, Kaynig V, Longair M, Pietzsch T, Preibisch S, Rueden C, Saalfeld S, Schmid B, Tinevez JY, White DJ, Hartenstein V, Eliceiri K, Tomancak P, Cardona A. Fiji: an open-source platform for biological-image analysis. *Nat Methods* 2012;**9**:676–82
40. Longair MH, Baker DA, Armstrong JD. Simple Neurite Tracer: open source software for reconstruction, visualization and analysis of neuronal processes. *Bioinformatics* 2011;**27**:2453–4
41. Binley KE, Ng WS, Tribble JR, Song B, Morgan JE. Sholl analysis: a quantitative comparison of semi-automated methods. *J Neurosci Methods* 2014;**225**:65–70
42. Baron R, Babcock AA, Nemirovsky A, Finsen B, Monsonego A. Accelerated microglial pathology is associated with Aβ plaques in mouse models of Alzheimer's disease. *Aging Cell* 2014;**13**:584–95
43. Powrozek TA, Olson EC. Ethanol-induced disruption of Golgi apparatus morphology, primary neurite number and cellular orientation in developing cortical neurons. *Alcohol* 2012;**46**:619–27
44. Faul F, Erdfelder E, Lang AG, Buchner A. G*Power 3: a flexible statistical power analysis program for the social, behavioral, and biomedical sciences. *Behav Res Methods* 2007;**39**:175–91
45. Alberini CM. Transcription factors in long-term memory and synaptic plasticity. *Physiol Rev* 2009;**89**:121–45
46. Göl MF, Erdoğan FF, Bayramov KK, Mehmetbeyoğlu E, Özkul Y. Assessment of genes involved in behavior, learning, memory, and synaptic plasticity following status epilepticus in rats. *Epilepsy Behav* 2019;**98**:101–9
47. Nonaka M, Kim R, Sharry S, Matsushima A, Takemoto-Kimura S, Bito H. Towards a better understanding of cognitive behaviors regulated by gene expression downstream of activity-dependent transcription factors. *Neurobiol Learn Mem* 2014;**115**:21–9
48. Sanders TH, Weiss J, Hogewood L, Chen L, Paton C, McMahan RL, Sweatt JD. Cognition-enhancing vagus nerve stimulation alters the epigenetic landscape. *J Neurosci* 2019;**39**:3454–69
49. Zovkic IB, Paulukaitis BS, Day JJ, Etikala DM, Sweatt JD. Histone H2A.Z subunit exchange controls consolidation of recent and remote memory. *Nature* 2014;**515**:582–6
50. Gensel JC, Schonberg DL, Alexander JK, McTigue DM, Popovich PG. Semi-automated Sholl analysis for quantifying changes in growth and differentiation of neurons and glia. *J Neurosci Methods* 2010;**190**:71–9
51. Williams PA, Thirgood RA, Oliphant H, Frizzati A, Littlewood E, Votruba M, Good MA, Williams J, Morgan JE. Retinal ganglion cell dendritic degeneration in a mouse model of Alzheimer's disease. *Neurobiol Aging* 2013;**34**:1799–806
52. Boscolo A, Ori C, Bennett J, Wiltgen B, Jevtovic-Todorovic V. Mitochondrial protectant pramipexole prevents sex-specific long-term cognitive impairment from early anaesthesia exposure in rats. *Br J Anaesth* 2013;**110**:i47–52
53. O'Mara SM, Commins S, Anderson M, Gigg J. The subiculum: a review of form, physiology and function. *Prog Neurobiol* 2001;**64**:129–55
54. Roy DS, Kitamura T, Okuyama T, Ogawa SK, Sun C, Obata Y, Yoshiki A, Tonegawa S. Distinct neural circuits for the formation and retrieval of episodic memories. *Cell* 2017;**170**:1000–219
55. Matsumoto N, Kitanishi T, Mizuseki K. The subiculum: unique hippocampal hub and more. *Neurosci Res* 2019;**143**:1–12
56. Joksimovic SM, DiGruccio MR, Boscolo A, Jevtovic-Todorovic V, Todorovic SM. The role of free oxygen radicals in lasting hyperexcitability of rat subicular neurons after exposure to general anesthesia during brain development. *Mol Neurobiol* 2020;**57**:208–16
57. Manzella FM, Joksimovic SM, Orfila JE, Fine BR, Dietz RM, Sampath D, Fiedler HK, Tesic V, Atluri N, Raol YH, Jevtovic-Todorovic V, Herson PS, Todorovic SM. Neonatal ketamine alters high-frequency oscillations and synaptic plasticity in the subiculum but does not affect sleep macrostructure in adolescent rats. *Front Syst Neurosci* 2020;**14**:26
58. Martínez-Cerdeño V. Dendrite and spine modifications in autism and related neurodevelopmental disorders in patients and animal models. *Dev Neurobiol* 2017;**77**:393–404
59. Sakamoto A, Imai J, Nishikawa A, Honma R, Ito E, Yanagisawa Y, Kawamura M, Ogawa R, Watanabe S. Influence of inhalation anesthesia assessed by comprehensive gene expression profiling. *Gene* 2005; **356**:39–48
60. Lin D, Liu J, Hu Z, Cottrell JE, Kass IS. Neonatal anesthesia exposure impacts brain microRNAs and their associated neurodevelopmental processes. *Sci Rep* 2018;**8**:10656
61. Cabrera OH, Useinovic N, Maksimovic S, Near M, Quillinan N, Todorovic SM, Jevtovic-Todorovic V. Neonatal ketamine exposure impairs infrapyramidal bundle pruning and causes lasting increase in excitatory synaptic transmission in hippocampal CA3 neurons. *Neurobiol Dis* 2022;**175**:105923
62. Pešić V, Milanović D, Popić J, Smiljanić K, Tešić V, Kanazir S, Jevtović-Todorović V, Ružđijić S. Neonatal propofol anesthesia modifies activity-dependent processes and induces transient hyperlocomotor

response to d-amphetamine during adolescence in rats. *Int J Dev Neurosci* 2015;**47**:266–77
63. Rial Verde EM, Lee-Osbourne J, Worley PF, Malinow R, Cline HT. Increased expression of the immediate-early gene arc/arg3.1 reduces AMPA receptor-mediated synaptic transmission. *Neuron* 2006;**52**:461–74
64. Shepherd JD, Rumbaugh G, Wu J, Chowdhury S, Plath N, Kuhl D, Huganir RL, Worley PF. Arc/Arg3.1 mediates homeostatic synaptic scaling of AMPA receptors. *Neuron* 2006;**52**:475–84
65. Penzes P, Cahill ME, Jones KA, VanLeeuwen JE, Woolfrey KM. Dendritic spine pathology in neuropsychiatric disorders. *Nat Neurosci* 2011;**14**:285–93
66. Gialloreti LE, Mazzone L, Benvenuto A, Fasano A, Alcon AG, Kraneveld A, Moavero R, Raz R, Riccio MP, Siracusano M, Zachor DA, Marini M, Curatolo P. Risk and protective environmental factors associated with autism spectrum disorder: evidence-based principles and recommendations. *J Clin Med* 2019;**8**:217
67. Huberman Samuel M, Meiri G, Dinstein I, Flusser H, Michaelovski A, Bashiri A, Menashe I. Exposure to general anesthesia may contribute to the association between cesarean delivery and autism spectrum disorder. *J Autism Dev Disord* 2019;**49**:3127–35
68. Laporta ML, Sprung J, Fejedelem CA, Henning DT, Weaver AL, Hanson AC, Schroeder DR, Myers SM, Voigt RG, Weingarten TN, Flick RP, Warner DO. Association between exposure of children to general anesthesia and autism spectrum disorder. *J Autism Dev Disord* 2022;**52**:4301–10
69. Ing C, Sun M, Olfson M, DiMaggio CJ, Sun LS, Wall MM, Li G. Age at exposure to surgery and anesthesia in children and association with mental disorder diagnosis. *Anesth Analg* 2017;**125**:1988–98
70. Song J, Li H, Wang Y, Niu C. Does exposure to general anesthesia increase risk of ADHD for children before age of three? *Front Psychiatry* 2021;**12**:717093
71. Tsai CJ, Lee CT, Liang SH, Tsai PJ, Chen VC, Gossop M. Risk of ADHD after multiple exposures to general anesthesia: a nationwide retrospective cohort study. *J Atten Disord* 2018;**22**:229–39
72. Sprung J, Flick RP, Katusic SK, Colligan RC, Barbaresi WJ, Bojanić K, Welch TL, Olson MD, Hanson AC, Schroeder DR, Wilder RT, Warner DO. Attention-deficit/hyperactivity disorder after early exposure to procedures requiring general anesthesia. *Mayo Clin Proc* 2012;**87**:120–9
73. Xu G, Strathearn L, Liu B, Yang B, Bao W. Twenty-year trends in diagnosed attention-deficit/hyperactivity disorder among US children and adolescents, 1997-2016. *JAMA Netw Open* 2018;**1**:e181471
74. Capocchi G, Zampolini M, Larson J. Theta burst stimulation is optimal for induction of LTP at both apical and basal dendritic synapses on hippocampal CA1 neurons. *Brain Res* 1992;**591**:332–6
75. Ishizuka N, Weber J, Amaral DG. Organization of intrahippocampal projections originating from CA3 pyramidal cells in the rat. *J Comp Neurol* 1990;**295**:580–623
76. Behr J, Gloveli T, Heinemann U. The perforant path projection from the medial entorhinal cortex layer III to the subiculum in the rat combined hippocampal-entorhinal cortex slice. *Eur J Neurosci* 1998;**10**:1011–8
77. Hutsler JJ, Zhang H. Increased dendritic spine densities on cortical projection neurons in autism spectrum disorders. *Brain Res* 2010;**1309**:83–94
78. Dark C, Homman-Ludiye J, Bryson-Richardson RJ. The role of ADHD associated genes in neurodevelopment. *Dev Biol* 2018;**438**:69–83
79. Yang T, Xiao T, Sun Q, Wang K. The current agonists and positive allosteric modulators of α7 nAChR for CNS indications in clinical trials. *Acta Pharm Sin B* 2017;**7**:611–22
80. Morley BJ, Mervis RF. Dendritic spine alterations in the hippocampus and parietal cortex of alpha7 nicotinic acetylcholine receptor knockout mice. *Neuroscience* 2013;**233**:54–63
81. McCann ME, de Graaff JC, Dorris L, Disma N, Withington D, Bell G, Grobler A, Stargatt R, Hunt RW, Sheppard SJ, Marmor J, Giribaldi G, Bellinger DC, Hartmann PL, Hardy P, Frawley G, Izzo F, von Ungern Sternberg BS, Lynn A, Wilton N, Mueller M, Polaner DM, Absalom AR, Szmuk P, Morton N, Berde C, Soriano S, Davidson AJ. Neurodevelopmental outcome at 5 years of age after general anaesthesia or awake-regional anaesthesia in infancy (GAS): an international, multicentre, randomised, controlled equivalence trial. *Lancet* 2019;**393**:664–77
82. Sun LS, Li G, Miller TL, Salorio C, Byrne MW, Bellinger DC, Ing C, Park R, Radcliffe J, Hays SR, DiMaggio CJ, Cooper TJ, Rauh V, Maxwell LG, Youn A, McGowan FX. Association between a single general anesthesia exposure before age 36 months and neurocognitive outcomes in later childhood. *JAMA* 2016;**315**:2312–20
83. Loomes R, Hull L, Mandy WPL. What is the male-to-female ratio in autism spectrum disorder? A systematic review and meta-analysis. *J Am Acad Child Adolesc Psychiatry* 2017;**56**:466–74
84. Mohammadi MR, Zarafshan H, Khaleghi A, Ahmadi N, Hooshyari Z, Mostafavi SA, Ahmadi A, Alavi SS, Shakiba A, Salmanian M. Prevalence of ADHD and its comorbidities in a population-based sample. *J Atten Disord* 2021;**25**:1058–67

(Received February 10, 2023, Accepted March 11, 2023)